ACS Catalysis

Research Article

Cite This: ACS Catal. 2019, 9, 9530−9538

pubs.acs.org/acscatalysis

Inverse Opal $CuCrO_2$ Photocathodes for H_2 Production Using Organic Dyes and a Molecular Ni Catalyst

Charles E. Creissen,[†] Julien Warnan,[†] Daniel Antón-García,[†] Yoann Farré,[‡] Fabrice Odobel,[‡] and Erwin Reisner*,[†]

[†]Christian Doppler Laboratory for Sustainable SynGas Chemistry, Department of Chemistry, University of Cambridge, Lensfield Road, Cambridge CB2 1EW, U.K.

[‡]Université LUNAM, Université de Nantes, CNRS, Chimie et Interdisciplinarité: Synthèse, Analyse, Modélisation (CEISAM), UMR 6230, 2 rue de la Houssinière, 44322 Nantes cedex 3, France

Supporting Information

ABSTRACT: Dye-sensitized photoelectrochemical (DSPEC) cells are an emerging approach to producing solar fuels. The recent development of delafossite $CuCrO_2$ as a p-type semiconductor has enabled H_2 generation through the coassembly of catalyst and dye components. Here, we present a $CuCrO_2$ electrode based on a high-surface-area inverse opal (IO) architecture with benchmark performance in DSPEC H_2 generation. Coimmobilization of a phosphonated diketopyrrolopyrrole (**DPP-P**) or perylene monoimide (**PMI-P**) dye with a phosphonated molecular Ni catalyst (**NiP**) demonstrates the ability of IO-$CuCrO_2$ to photogenerate H_2. A positive photocurrent onset potential of approximately +0.8 V vs RHE was achieved with these photocathodes. The **DPP-P**-based photoelectrodes delivered photocurrents of −18 μA cm^{-2} and generated 160 ± 24 nmol of H_2 cm^{-2}, whereas the **PMI-P**-based photocathodes displayed higher photocurrents of −25 μA cm^{-2} and produced 215 ± 10 nmol of H_2 cm^{-2} at 0.0 V vs RHE over the course of 2 h under visible light illumination (100 mW cm^{-2}, AM 1.5G, λ > 420 nm, 25 °C). The high performance of the PMI-constructed system is attributed to the well-suited molecular structure and photophysical properties for p-type sensitization. These precious-metal-free photocathodes highlight the benefits of using bespoke IO-$CuCrO_2$ electrodes as well as the important role of the molecular dye structure in DSPEC fuel synthesis.

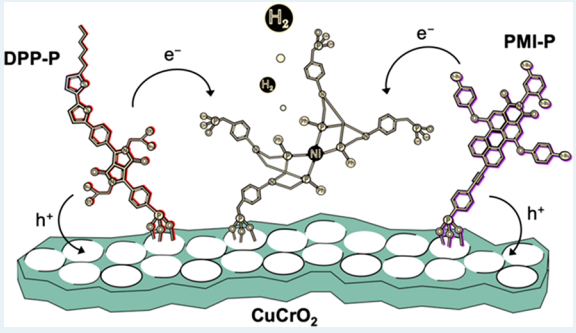

KEYWORDS: *dye-sensitized, molecular catalyst, photocatalysis, solar fuels, p-type semiconductor, delafossite*

INTRODUCTION

Solar conversion of water into chemical energy carriers offers a sustainable alternative to fossil fuels.[1−3] Dye-sensitized photoelectrochemical (DSPEC) cells featuring molecular catalysts are a promising technology for solar water splitting due to their engineering flexibility, easy modification, and assembly.[4−8] In these systems, semiconductor-immobilized molecular dyes harvest solar light and transfer charge to a catalytic site, facilitating the synthesis of solar fuels. Significant progress with dye-sensitized photocathodes (DSPCs) and photoanodes has been made possible through a deeper understanding of charge transfer processes and performance-limiting recombination routes.[9−18] Although efficiency has improved in recent years, DSPCs still suffer from low photocurrents and poor catalytic activity, representing a bottleneck in state of the art DSPEC devices.

In DSPCs, light absorption by the dye is typically followed by hole injection into the semiconductor, creating a reduced dye that can transfer an electron to the coimmobilized catalyst. The steady-state photocurrent is representative of the kinetic interplay between productive charge transfer and detrimental recombination pathways. Therefore, higher photocurrents can be achieved by blocking the dominant recombination mechanisms between holes in the p-type semiconductor and (1) the reduced dye (geminate recombination) or (2) the reduced catalyst.[19−25]

Methods to minimize catalyst recombination in DSPCs through layer-by-layer assemblies[26−29] and molecular dye−catalyst dyad complexes[30−37] have shown some success, but the photocatalytic activity is still limited. Modular assembly through a coimmobilization route is generally preferred, as it provides flexibility in the construction of the electrode, avoiding complex synthetic modification and permitting the use of already established molecular species.[38] The undesirable geminate recombination pathway can be rationally addressed through engineering of the dye structure. Charge transfer from an immobilized dye to a semiconductor is highly dependent on the spatial separation.[39−43] Consequently, localizing charge

Received: July 15, 2019
Revised: September 4, 2019
Published: September 9, 2019

DOI: 10.1021/acscatal.9b02984
ACS Catal. 2019, 9, 9530−9538

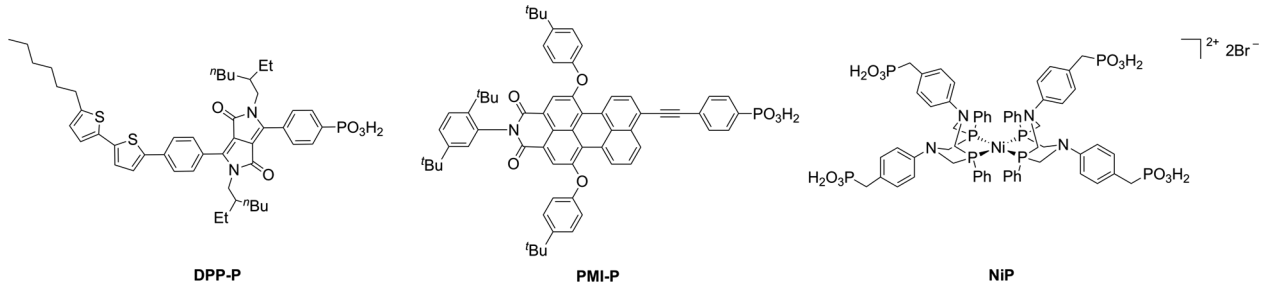

Figure 1. Chemical structures of molecular dyes **DPP-P** and **PMI-P** and molecular H_2 evolution catalyst **NiP** used in this study.

density in the photoreduced dye (i.e., the ground state LUMO) away from the semiconductor surface reduces charge recombination kinetics. Such strategies have proven beneficial in p-type dye-sensitized solar cells (p-DSSCs) to effectively increase the photocurrent and photovoltage.[16,44,45] In particular, organic dyes have proven to be proficient rivals to conventional precious-metal dyes, commonly displaying favorable qualities for p-type sensitization such as high extinction coefficients and internal acceptor units.[16,46−48] The two dyes used in this study are based on diketopyrrolopyrrole (DPP) and perylene monoimide (PMI) chromophores, both of which exhibit beneficial characteristics for incorporation in DSPCs.

Nonetheless, the key component in both recombination routes is the semiconductor. NiO is currently the dominant wide-bandgap p-type semiconductor in DSPCs owing to simple preparation using solution-based techniques.[26,49−52] However, problems associated with the high density of traps and low hole mobility have been identified,[53−55] which account for the scarcity of reports of H_2 generation with coimmobilized dye and catalyst components.[20,21,38,56−59] Improved DSPCs can be realized through the development of alternative wide-bandgap p-type semiconductors. Delafossite structures are suitable candidates due to their solution processability, high hole mobility, and metal oxide character.[60−63] $CuGaO_2$ and $CuCrO_2$ have been employed in DSPCs, both enabling an early photocurrent onset due to their highly anodic valence band positions.[32,64−66] In particular, $CuCrO_2$ formed using a sol−gel method was able to generate H_2 in a coimmobilized molecular dye/catalyst assembly.[64] The DSPC outperformed an analogous NiO-based photocathode, but low dye and catalyst loadings limited product generation. This issue can in principle be addressed through development of meso- and macroporous architectures such as inverse opal (IO) structures, which has previously proven effective for the incorporation of dye and catalyst components on metal oxides.[27,28,67−75]

Here, IO-$CuCrO_2$ electrodes are reported through a bottom-up templating method using organic microsphere templates and delafossite $CuCrO_2$ particles. Two organic dyes (**DPP-P**[76] and **PMI-P**,[77] Figure 1) were explored in this study and coimmobilized with a DuBois-type molecular Ni catalyst[78−82] (**NiP**, Figure 1). Photoelectrochemical (PEC) H_2 generation was used to demonstrate the influence of the novel $CuCrO_2$ morphology and dye structure on performance.

RESULTS AND DISCUSSION

Synthesis and Characterization of IO-$CuCrO_2$ Electrodes. IO-$CuCrO_2$ electrodes were constructed using a bottom-up templating method using mixtures of preformed $CuCrO_2$ nanoparticles (NPs) with polystyrene (PS) beads (750 nm diameter). $CuCrO_2$-NPs were synthesized using a modified hydrothermal synthesis procedure.[83] In brief, $Cu(NO_3)_2{\cdot}3H_2O$ (6.25 mmol) and $Cr(NO_3)_3{\cdot}9H_2O$ (6.25 mmol) were stirred in Milli-Q H_2O (70 mL) and NaOH (5 g) was added. The resulting alkaline solution was placed in a PTFE-lined autoclave and heated to 240 °C for 60 h. The NPs were washed consecutively with dilute HCl and EtOH three times and then dried in vacuo. Transmission electron microscopy (TEM) analysis showed that crystalline particles of approximately 15 nm in length and 5 nm in diameter were obtained (Figure S1) with a Brunauer−Emmett−Teller (BET) surface area of 86 $m^2\ g^{-1}$. Powder X-ray diffraction (XRD) analysis confirmed the 3R delafossite structure (Figure S2).

The $CuCrO_2$-NPs were dispersed in a 4/1 H_2O/MeOH mixture through sonication. The PS beads were washed with MeOH, and a portion of the $CuCrO_2$-NP mixture was added. The dispersion was sonicated and drop-cast on precleaned ITO-coated glass confined to a circular area with Parafilm and left to dry under ambient conditions. The Parafilm was removed, and the PS template was dissolved in toluene. The films were subsequently washed with acetone and dried before being sintered at 500 °C for 1 h under argon. Scanning electron microscopy (SEM) analysis showed that the IO-$CuCrO_2$ films were approximately 2 μm thick with macropores roughly 600−700 nm in diameter (Figure 2a,b). XRD patterns of the IO-$CuCrO_2$ films displayed peaks consistent with the 3R delafossite polytype (Figure S2).

Dye and Catalyst Properties. **DPP-P**,[76] **PMI-P**,[77] and **NiP**[78] were synthesized as previously reported. The phosphonic acid anchoring groups facilitate immobilization on metal oxide surfaces, and both dyes have previously been employed in colloidal dye-sensitized photocatalysis systems with TiO_2-NPs and **NiP** using sacrificial reagents.[76,77,84] **DPP-P** was previously shown to be an effective dye in a $CuCrO_2$ photocathode with **NiP** and is therefore a suitable choice for comparative purposes in this study.[64] PMI dyes are renowned for their high stability and intense visible light absorption.[45] PMI-based photocathodes have been established with heterogeneous catalysts[85] and with molecular catalysts in solution,[86] but no examples with an immobilized molecular catalyst currently exist.

The two dyes exhibit similar electrochemical properties in solution (Table S1). Importantly, both dye anions exhibit sufficient thermodynamic driving force ($E_{dye/dye^-} \approx -0.7$ V vs RHE) to reduce **NiP** to a catalytically active state ($E_{NiP,onset} = -0.21$ V vs RHE).[78] Hole injection into the valence band of $CuCrO_2$ ($E_{fb} \approx +1.0$ V vs RHE) is facilitated by the highly anodic excited state reduction potentials ($E_{DPP\text{-}P^*/DPP\text{-}P^-} = +1.57$ V vs RHE and $E_{PMI\text{-}P^*/PMI\text{-}P^-} = +1.47$ V vs RHE).[64,87] **PMI-P** displays a broad and intense absorption signal from 450

DOI: 10.1021/acscatal.9b02984
ACS Catal. 2019, 9, 9530−9538

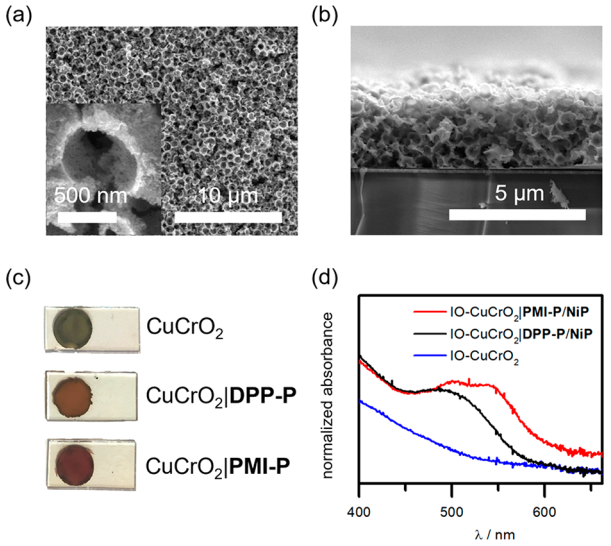

Figure 2. (a) Top-down and (b) cross-sectional SEM images of IO-$CuCrO_2$ electrodes. (c) Photographs and (d) diffuse reflectance UV–vis spectra of the dye- and catalyst-loaded electrodes.

to 600 nm with a maximum at 536 nm (ε_{max} = 3.8 × 10^4 M^{-1} cm^{-1}, E_{00} = 2.20 eV) and a shoulder at 500 nm in solution-based UV–vis spectra. **DPP-P** also displays a broad absorption signal (425–550 nm) with a maximum centered at 496 nm (ε_{max} = 2.6 × 10^4 M^{-1} cm^{-1}, E_{00} = 2.27 eV) (Figure S3).

The intense visible light absorption and favorable electrochemical properties for both dyes are well-suited for application in DSPCs with **NiP** as the catalyst. To assess their ability to reduce the immobilized catalyst, photocathodes were assembled for PEC analysis.

Photocathode Assembly. Photocathodes were constructed through sequential anchoring of the dye followed by the catalyst. IO-$CuCrO_2$ electrodes were soaked in a solution of **PMI-P** or **DPP-P** (0.2 mM, DMF, 15 h) before rinsing with DMF and then H_2O. The resulting IO-$CuCrO_2$|dye electrodes were dried under N_2 and then immersed in a **NiP** solution (1 mM, MeOH, 3 h) under a N_2 atmosphere to form IO-$CuCrO_2$|dye/**NiP** electrodes (see the Experimental Section for details).

The color of the IO-$CuCrO_2$ electrodes changed from light green to red or orange for the **PMI-P**- or **DPP-P**-sensitized electrodes, respectively (Figure 2c). UV–vis spectra of the films showed the characteristic visible light absorption profiles of the dyes. IO-$CuCrO_2$|**PMI-P** electrodes displayed higher intensity for the peak at 500 nm than at 536 nm as opposed to the solution-based experiments—this could be attributed to the underlying absorption of $CuCrO_2$ or to the presence of aggregates (Figure 2d).[77,88]

The loading of each dye was quantified following desorption in basic solution by electronic absorption spectrophotometry, and the amount of catalyst was determined using inductively coupled plasma-optical emission spectroscopy (ICP-OES) (Table S2). The high-surface-area IO-$CuCrO_2$ electrodes loaded approximately 20 nmol cm^{-2} of the combined molecular species with a dye/catalyst ratio of approximately 3/1. The loading corresponds to a 5-fold increase over the previously reported sol–gel $CuCrO_2$ electrodes (loading approximately 4 nmol cm^{-2}).[64]

Photoelectrochemical H_2 Generation. PEC analysis was conducted in aqueous Na_2SO_4 solution (0.1 M, pH 3) under chopped visible light illumination (100 mW cm^{-2}, AM 1.5G, λ > 420 nm). Mildly acidic conditions are optimal for the catalytic H_2 generation performance of **NiP**.[78,89,90] Linear sweep voltammograms (LSVs) showed that cathodic photocurrents were obtained for IO-$CuCrO_2$|**DPP-P/NiP** and IO-$CuCrO_2$|**PMI-P/NiP** electrodes with an onset potential of approximately +0.8 V vs RHE (Figure 3a). Chronoamperometry analysis conducted at 0.0 V vs RHE displayed higher photocurrents for the **PMI-P** photocathodes ($j \approx -25$ μA cm^{-2}) than the corresponding **DPP-P** electrodes ($j \approx -18$ μA cm^{-2}) (Figure 3b). The enhancement can be assigned to the red-shifted, more intense, and broader absorption profile of the PMI dye.

Transient photocurrent spikes were observed for both photocathodes, which are representative of charge accumulation at the semiconductor/electrolyte solution interface. Previous systems have also associated such spikes with recombination,[36,91] but the exact origin is not easily identifiable because both dominant recombination routes can contribute to the effect. In this study, the **PMI-P**-based photocathodes generate the highest cathodic spikes, suggesting substantial charge accumulation at the interface. Kinetic modeling could provide further insight into the exact mechanism and has been successfully applied in similar systems[92] but is beyond the scope of the current study.

All electrodes displayed a dark current previously assigned to a $Cu^{II/I}$ redox couple and associated oxygen intercalation in LSVs.[64,93] Interestingly, the dark current decreased upon immobilization of the individual dye and catalyst components

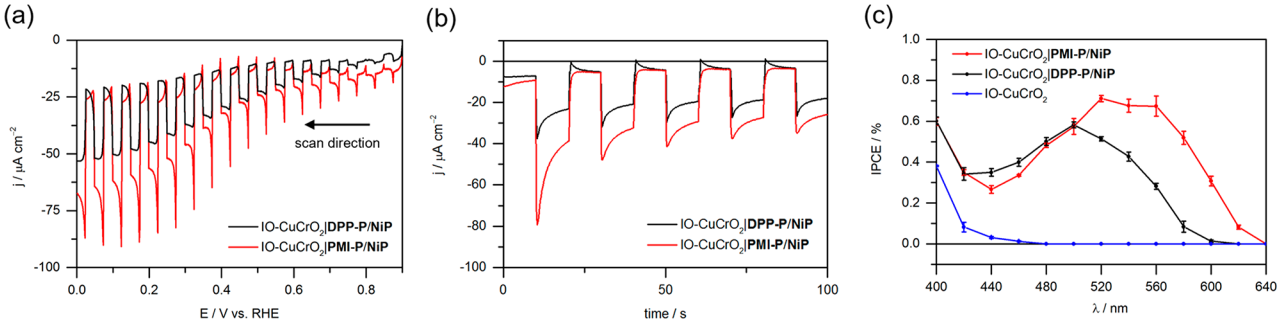

Figure 3. (a) LSVs and (b) chronoamperometry analysis of IO-$CuCrO_2$ electrodes at 0.0 V vs RHE. (c) IPCE plots of IO-$CuCrO_2$ electrodes at +0.3 V vs RHE with monochromatic light intensity maintained at 0.8 mW cm^{-2}. Conditions (a–c): aqueous Na_2SO_4 (0.1 M, pH 3), chopped visible light illumination (100 mW cm^{-2}, AM 1.5G, λ > 420 nm), scan rate 5 mV s^{-1} for voltammograms, 25 °C cell temperature maintained. A geometric electrode area of 0.25 cm^2 was used for all experiments.

DOI: 10.1021/acscatal.9b02984
ACS Catal. 2019, 9, 9530–9538

(Figure S4) and the same effect was observed upon anchoring of an insulating organic molecule (phenylphosphonic acid) (Figure S5). The result agrees with a likely binding mechanism through M−O−P bonds,[94] which shields the Cu sites from the electrolyte solution, thus lowering the observed redox signal.

Incident photon-to-current conversion efficiency (IPCE) measurements resembled the UV−vis spectra for each dye (Figure 3c). The inversion in peak maxima for the IO-$CuCrO_2$|**PMI-P**/**NiP** photocathodes in comparison with the solution absorption suggests that aggregates contribute to photocurrent in this arrangement. Although often associated with adverse effects, aggregation due to $\pi-\pi$ stacking of PMI units in related dye-sensitized systems has recently been shown to mediate charge separation on long time scales.[95] A similar effect relating to charge accumulation on the PMI units could favor charge transfer and contribute to the photocurrent in this case. The higher values for **PMI-P** electrodes are representative of higher catalytic activity due to the greater degree of visible light absorption.

Controlled-potential photoelectrolysis (CPPE) was required to confirm the origin of the photocurrent. CPPE experiments were conducted with each electrode at applied potentials of 0.0 and +0.3 V vs RHE in aqueous Na_2SO_4 (0.1 M, pH 3) over the course of 2 h under constant light illumination (100 mW cm^{-2}, AM 1.5G, $\lambda > 420$ nm) (Table 1 and Figure S6). IO-$CuCrO_2$|**DPP-P**/**NiP** and IO-$CuCrO_2$|**PMI-P**/**NiP** photocathodes generated appreciable amounts of H_2 at each applied potential, with the highest activity observed at 0.0 V vs RHE. IO-$CuCrO_2$|**PMI-P**/**NiP** electrodes generated 215 ± 10 nmol of H_2 cm^{-2} with a Faradaic efficiency (FE) of 41 ± 8%, giving a turnover number for **NiP** (TON_{NiP}) of 48 ± 2. IO-$CuCrO_2$|**DPP-P**/**NiP** showed slightly lower performance, generating 160 ± 24 nmol of H_2 cm^{-2} with a FE of 40 ± 14% and a TON_{NiP} of 36 ± 5. No H_2 was detected for IO-$CuCrO_2$, IO-$CuCrO_2$|dye, or IO-$CuCrO_2$|**NiP** electrodes, confirming the need for both dye and catalyst molecules for catalysis. These control experiments also rule out any contribution from electrode-derived heterogeneous catalysts as previously observed in other systems.[96] The modest FE is at least partially attributed to the persistent dark current originating from the $Cu^{II/I}$ redox couple.[64,93]

Table 1. PEC H_2 Generation with Corresponding TON_{NiP} and FE for IO-$CuCrO_2$|PMI-P/NiP and IO-$CuCrO_2$|DPP-P/NiP Photocathodes at Different Applied Potentials over the Course of 2 h[a]

	H_2 (nmol cm^{-2})	TON_{NiP}	FE (%)
IO-$CuCrO_2$|**PMI-P**/**NiP**			
+0.3 V vs RHE	184 ± 22	41 ± 5	45 ± 6
+0.0 V vs RHE	215 ± 10	48 ± 2	41 ± 8
IO-$CuCrO_2$|**DPP-P**/**NiP**			
+0.3 V vs RHE	72 ± 9	16 ± 2	25 ± 1
+0.0 V vs RHE	160 ± 24	36 ± 5	40 ± 14

[a]Conditions: aqueous Na_2SO_4 (0.1 M, pH 3), UV-filtered simulated solar light (100 mW cm^{-2}, AM 1.5G, $\lambda > 420$ nm, 25 °C), geometrical surface area of 0.25 cm^2. TON_{NiP} was calculated using the catalyst loading determined from ICP-OES measurements.

Postcatalysis ICP-OES showed that approximately 85% and 75% of the initial **NiP** loaded was retained on the surface of IO-$CuCrO_2$|**PMI-P**/**NiP** and IO-$CuCrO_2$|**DPP-P**/**NiP** electrodes, respectively (Table S2). Corresponding sol−gel derived IO-$CuCrO_2$|**DPP-P**/**NiP** photocathodes preserved only 50% of the catalyst, suggesting that the immobilized **NiP** is stabilized against desorption by the IO-$CuCrO_2$ structures.

Comparison with State of the Art. The photocathodes presented here display high activities for coimmobilized molecular DSPCs. Incorporation of a coumarin 343 dye coimmobilized with a bimetallic iron-based catalyst on NiO generated photocurrents of −10 μA cm^{-2} at +0.16 V vs RHE with a FE of 50% but was extremely short lived due to degradation of the catalyst with a final TON ≤ 3.[57] A cobalt diimine-dioxime system featuring a coanchored push−pull dye on NiO generated photocurrents of −7.5 μA cm^{-2} at +0.14 V vs RHE, producing H_2 with an FE of 10%.[38] Immobilization of the same push−pull dye with a cobaloxime catalyst on $CuGaO_2$ boosted H_2 generation, increasing the FE to 74%; this further stresses the importance of altering the semiconductor unit in DSPCs.[66] The high photocurrents, FEs, and TONs of the **PMI-P** (−25 μA cm^{-2}, FE = 41%, TON = 48) and **DPP-P** (−18 μA cm^{-2}, FE = 40%, TON = 36) photocathodes presented here highlight the benefits of using $CuCrO_2$. Furthermore, the first example of a PMI-sensitized DSPC with an immobilized molecular catalyst is presented. The high performance of the PMI system directs research toward modification of similar chromophores that benefit from high extinction coefficients and favorable structural properties for sensitization of p-type semiconductors.

NiP has previously been incorporated as the catalyst in DSPCs. Layer-by-layer assembly of a phosphonated Ru-polypyridyl dye and **NiP** on NiO using a Zr^{IV} linker facilitated H_2 generation but with low activity.[26] Incorporation of a donor−dye−catalyst assembly with a Ru-based dye reported photocurrents of −56 μA cm^{-2} at +0.05 V vs RHE with a TON of ∼16 and an FE of 53%.[27] A subsequent trilayered NiO/ITO assembly without the donor assembly enhanced the FE to 90%.[28] The PMI and DPP photocathodes in the current study avoid precious-metal components but retain high activity. Although not as efficient as the best Ru-dye **NiP**-based examples, they are competitive despite the simple coimmobilization strategy. Layer-by-layer assemblies using organic dyes with $CuCrO_2$ could further reduce catalyst recombination to enhance activity in future studies.

The benefits of modifying NiO through doping and defect passivation/elimination has been outlined in previous reports.[28,97,98] Similar improvements to $CuCrO_2$ electrodes are expected to result in enhanced performance. Here, the development of our previous $CuCrO_2$ system through altering the semiconductor morphology increased photocurrents and product yields. The amount of H_2 generated is 70% higher with the IO-$CuCrO_2$ electrodes, the enhanced performance being assigned to higher molecular loadings (500% increase) of dye and catalyst in the extended IO network. The sustained photocurrent of the IO-$CuCrO_2$ photocathode is approximately twice that of the previous $CuCrO_2$ system; however, the lower TON achieved is likely due to a significant amount of each species that is grafted on the electrode but does not contribute to catalysis. Significant light scattering/absorption of the IO films is another likely cause, where light harvesting from dye molecules buried within the film is highly limited. The issue could be addressed through pore size modification and thickness control to rationally tailor the IO network for a specific dye/catalyst combination without significantly reducing the molecular loading. Similar approaches to increase the

DOI: 10.1021/acscatal.9b02984
ACS Catal. 2019, 9, 9530−9538

surface area could prove effective with other p-type semiconductors in future studies.

The advantage of bypassing synthetically challenging complexes through coimmobilization increases the diversity of available photocathodes. Well-studied organic chromophores such as the two employed here can be integrated with the established range of Earth-abundant molecular catalysts,[1] enabling inexpensive and efficient reduction reactions. Future developments of dye−catalyst assemblies based on IO-$CuCrO_2$ could provide an understanding of the catalysis-limiting processes in DSPCs.

CONCLUSIONS

We report two inverse opal $CuCrO_2$ photocathodes using different organic dyes with a coimmobilized molecular Ni bis(diphosphine) catalyst. The IO architecture enables high loadings of molecular species, resulting in a 70% enhancement in H_2 generation over a previously reported analogous sol−gel $CuCrO_2$ photocathode. This PMI-sensitized $CuCrO_2$ electrode benefits from a broad and intense absorption profile, ensuring that a large portion of visible light can be effectively harvested. Both IO-$CuCrO_2$|**PMI-P**/**NiP** and IO-$CuCrO_2$|**DPP-P**/**NiP** photocathodes generate photocurrents of −25 and −18 μA cm^{-2}, respectively, at 0.0 V vs. RHE under visible light illumination (100 mW cm^{-2}, AM 1.5G, λ > 420 nm). The photocurrent onset potential was approximately +0.8 V vs RHE for both architectures. **DPP-P**- and **PMI-P**-sensitized photocathodes produce appreciable amounts of H_2 over the course of 2 h CPPE. The IO-$CuCrO_2$|**PMI-P**/**NiP** photoelectrodes perform best, producing 215 ± 10 nmol of H_2 cm^{-2} at 0.0 V vs RHE with an FE of 41 ± 8% and a TON_{NiP} of 48 ± 2. Under the same conditions, IO-$CuCrO_2$|**DPP-P**/**NiP** generates 160 ± 24 nmol of H_2 cm^{-2} with a FE of 40 ± 14% and a TON_{NiP} of 36 ± 5. The high performance of **PMI-P** reflects the favorable molecular structure and absorption spectrum, which is well-suited for sensitization of p-type semiconductors.

The novel IO-$CuCrO_2$ morphology emphasizes the importance of high-surface-area structures and more suitable p-type semiconductors in DSPCs. Coimmobilization of catalyst and dye components proves to be a viable method to form DSPCs with $CuCrO_2$, avoiding the need for a complicated synthetic protocol. Furthermore, the procedure enables control over pore size through the use of different-sized template spheres, which could assist the development of DSPCs in future studies. Integration of CO_2 reduction catalysts and development of dyes tailored for this $CuCrO_2$ surface could provide vital advancements for delafossite-based photocathodes. The novel and transferable IO-$CuCrO_2$ structure presented here extends the range of materials available for fuel-generating DSPCs.

EXPERIMENTAL SECTION

Materials and Methods. **NiP**,[78] **DPP-P**,[76] and **PMI-P**[77] were synthesized as previously reported. Milli-Q H_2O (R > 18.2 MΩ cm) was used for all electrochemical and analytical measurements. $Cu(NO_3)_2{\cdot}3H_2O$ (Sigma-Aldrich, ≥99%), $Cr(NO_3)_3{\cdot}9H_2O$ (Sigma-Aldrich, ≥99%), and anhydrous NaOH pellets (Sigma-Aldrich, ≥98%) were used for the $CuCrO_2$-NP preparation.[83] PS beads (Polysciences Inc., 750 nm, 2.6% w/v) were used for IO-$CuCrO_2$ synthesis. ITO-coated glass sheets (Vision Tek Systems Ltd., R = 12 Ω cm^{-2}, thickness of 1.1 mm) were cut into 1 × 3 cm^2 slides prior to cleaning.

Synthesis of $CuCrO_2$-NPs. $Cu(NO_3)_2{\cdot}3H_2O$ (1.51 g, 6.25 mmol) and $Cr(NO_3)_3{\cdot}9H_2O$ (2.50 g, 6.25 mmol) were stirred in Milli-Q H_2O (70 mL), and NaOH (5.0 g) was added (final solution pH 13). The solution was stirred at room temperature for 2 h, and then 12 mL was decanted into a PTFE-lined autoclave (23 mL total volume). The autoclave was heated to 240 °C for 60 h before the $CuCrO_2$-NPs were removed. The particles were washed with HCl (0.1 M, 15 mL) and centrifuged (8000 rpm, 5 min), and the supernatant was removed. They were then washed with EtOH (15 mL) and recentrifuged, and the supernatant was removed. The washing steps were repeated for a total of three washes before the $CuCrO_2$-NPs were dried in vacuo. The dry NPs were ground using a pestle and mortar and stored under vacuum before use.

Synthesis of IO-$CuCrO_2$ Electrodes. PS beads (750 nm, 2.6% w/v suspension in H_2O, 0.5 mL) were centrifuged, and the supernatant was removed; the beads were then washed with MeOH and centrifuged again to give a PS pellet. A dispersion of $CuCrO_2$-NPs (7.5 wt %, MeOH/H_2O 1/4, 140 μL) was added to the PS pellet and sonicated (5 min at <10 °C). The solution was drop-cast (4 μL) on ITO-coated glass (0.5 cm^2, confined with Parafilm) and dried in air for 3 h. The Parafilm was removed and the PS template dissolved in toluene for 15 h before being rinsed with acetone then H_2O and dried in vacuo. Annealing under Ar (500 °C, 5 °C min^{-1} ramp rate, 1 h, 150 sccm flow rate) using a tube furnace fitted with a quartz tube, end seals, and insulation plugs (Carbolite Gero) was required to sinter the particles to form the final IO-$CuCrO_2$ structures.

Physical Characterization. A Tescan MIRA3 FEG-SEM was used to obtain all SEM images. TEM analysis was conducted using a FEI Phillips Technai F20-G2 TEM, operating at an accelerating voltage of 200 kV (Electron Microscopy Suite, Cavendish Laboratory, University of Cambridge). XRD measurements were taken with a PANalytical BV X'Pert Pro X-ray diffractometer. UV−vis absorption spectra were acquired using a Varian Cary 50 spectrophotometer operated in transmission mode or with a diffuse reflectance accessory (Barrelino) for powder samples. Emission spectra were recorded on a Fluoromax-4 Horiba Jobin Yvon spectrofluorimeter (PMI) or with an Edinburgh Instruments FS5 spectrofluorimeter (DPP). N_2 gas adsorption measurements were carried out using a Micromeritics 3 Flex instrument (Micromeritics, Norcross, GA, USA) with powder samples. Samples were degassed for 10 h at 100 °C, and measurements were carried out in liquid N_2. BET specific surface area values were obtained from fitting N_2 isotherms using the Microactive software.

Immobilization of Dyes and Catalyst. The dye species were immobilized through soaking in a bath containing **DPP-P** or **PMI-P** (0.2 mM) for 15 h in DMF, maintained at 25 °C. The IO-$CuCrO_2$|dye electrodes were rinsed with DMF and water before being dried under N_2. These electrodes were then soaked in **NiP** (1 mM, MeOH) for 3 h under a N_2 atmosphere. The IO-$CuCrO_2$|dye/**NiP** electrodes were rinsed with MeOH and then water and dried under N_2 in the dark. All electrodes were used directly after immobilization. A bare IO-$CuCrO_2$ electrode was soaked in a solution of phenylphosphonic acid (0.5 M, DMF) for 2 h and then rinsed with DMF and H_2O for the comparative dark current study.

DOI: 10.1021/acscatal.9b02984
ACS Catal. 2019, 9, 9530−9538

Quantification of Immobilized DPP-P and NiP. **DPP-P** and **PMI-P** loadings were quantified using UV−vis spectroscopy following desorption from IO-$CuCrO_2$|dye/**NiP** electrodes by scraping the $CuCrO_2$-NP powder from the surface (0.25 cm^2) and sonicating in tetrabutylammonium hydroxide (TBAOH) 30-hydrate (0.1 M, DMF, 1 mL) for 30 min. Higher TBAOH concentrations and longer sonication times were avoided to prevent dye decomposition. The absorption maximum at 500 and 536 nm for **DPP-P** and **PMI-P** electrodes, respectively, was determined and fitted to a calibration curve (conducted in 0.1 M TBAOH in DMF) to determine the loading values. **NiP** loading was determined by ICP-OES following overnight digestion of the electrodes (0.25 cm^2) in aqueous HNO_3 (70%, 1 mL) and subsequent dilution to 10% v/v with Milli-Q H_2O. Values for nitric acid solution, IO-$CuCrO_2$, IO-$CuCrO_2$|**DPP-P**, IO-$CuCrO_2$|**PMI-P**, and pre- and postelectrolysis $CuCrO_2$|**DPP-P**/**NiP** and $CuCrO_2$|**PMI-P**/**NiP** electrodes were determined in triplicate.

Photoelectrochemical Measurements. PEC measurements were conducted using an Ivium CompactStat potentiostat in a custom two-compartment electrochemical cell featuring a flat quartz window and a Nafion membrane. A three-electrode setup was used with a Pt counter electrode, Ag/AgCl/KCl_{sat} reference electrode, and an IO-$CuCrO_2$-based working electrode (0.25 cm^2 active area). N_2-purged (15 min) aqueous Na_2SO_4 electrolyte solution (0.1 M, pH 3) was used for all measurements. Electrodes were illuminated from the front using a calibrated Newport Oriel solar light simulator (150 W, 100 mW cm^{-2}, AM 1.5G) with an IR water filter and a UQG Optics UV-Filter (λ > 420 nm).

CPPE experiments with each photocathode were conducted in triplicate at +0.3 and 0.0 V vs RHE in a custom two-compartment electrochemical cell featuring a flat quartz window and a Nafion membrane. Both compartments were purged with 2% CH_4 in N_2 for 30 min prior to electrolysis, and the amount of H_2 was determined using a Shimadzu Tracera GC2010 Plus gas chromatograph using a barrier ionization discharge detector and a molsieve column (kept at 130 °C) with He as the carrier gas. All PEC cells were left for 2 h following electrolysis to allow solution-dissolved H_2 to equilibrate with the gas headspace. The partial pressure of H_2 was calculated to account for dissolved gas in the solution, and this was added to the amount of H_2 in the headspace to determine the total H_2 and Faradaic efficiency.

IPCE Measurements. A three-electrode setup with a Pt counter electrode, Ag/AgCl/KCl_{sat} reference electrode, and an IO-$CuCrO_2$|dye/**NiP** or IO-$CuCrO_2$ working electrode was used in a custom three-necked cell with a flat borosilicate glass window for IPCE measurements. The electrolyte solution was Na_2SO_4 (0.1 M, pH 3), and an applied potential of +0.3 V vs RHE was maintained for all measurements. Monochromatic light was supplied with a 300 W xenon lamp solar light simulator connected to a monochromator (MSH300, LOT Quantum design). The intensity was calibrated to 0.8 mW cm^{-2} for each individual wavelength, and experiments with each electrode were conducted in triplicate with different electrodes using an active area of 0.25 cm^2. Photocurrents were determined at each recorded wavelength through light chopping using an Ivium CompactStat potentiostat. Error bars represent standard deviation from the mean.

■ ASSOCIATED CONTENT

Supporting Information

The Supporting Information is available free of charge on the ACS Publications website at DOI: 10.1021/acscatal.9b02984.

Additional figures and tables as described in the text (PDF)

■ AUTHOR INFORMATION

Corresponding Author

*E-mail for E.R.: reisner@ch.cam.ac.uk.

ORCID

Fabrice Odobel: 0000-0001-7289-4160

Erwin Reisner: 0000-0002-7781-1616

Author Contributions

All authors have given approval to the final version of the manuscript.

Notes

The authors declare no competing financial interest.

Data related to this publication are available at the University of Cambridge data repository: https://doi.org/10.17863/CAM.43804.

■ ACKNOWLEDGMENTS

The work presented was supported by the Christian Doppler Research Association (Austrian Federal Ministry for Digital and Economic Affairs and the National Foundation for Research, Technology and Development), the OMV Group (E.R., C.E.C., and J.W.), the EPSRC NanoDTC in Cambridge (EP/L015978/1; E.R. and C.E.C.), and an EPSRC PhD DTA studentship (EP/M508007/1; D.A.-G.). We thank Laura Healy (Department of Geography, University of Cambridge) for ICP-OES measurements. We are grateful to Agence Nationale de la Recherche (ANR) for financial support of this research through the program POSITIF (ANR-12-PRGE-0016-01) and Région des Pays de la Loire for the project LUMOMAT (F.O. and Y.F.). We appreciate suggestions and comments on the manuscript from Esther Edwardes Moore and Dr. Souvik Roy.

■ ABBREVIATIONS

ITO, indium tin oxide; ICP-OES, inductively coupled plasma-optical emission spectrometry; SEM, scanning electron microscopy; E_{fb}, flatband potential; BET, Brunauer-Emmett-Teller; XRD, X-ray diffraction; LSV, linear sweep voltammetry; RHE, reversible hydrogen electrode; LUMO, lowest unoccupied molecular orbital; TBAOH, tetrabutylammonium hydroxide; DSPEC, dye-sensitized photoelectrochemical; IO, inverse opal; DSPC, dye-sensitized photocathode; p-DSSC, p-type dye-sensitized solar cell; DPP, diketopyrrolopyrrole; PMI, perylene monoimide; PEC, photoelectrochemical; NP, nanoparticle; PS, polystyrene; IPCE, incident photon-to-current conversion efficiency; CPPE, controlled potential photoelectrolysis; FE, Faradaic efficiency; TON, turnover number

■ REFERENCES

(1) Dalle, K. E.; Warnan, J.; Leung, J. J.; Reuillard, B.; Karmel, I. S.; Reisner, E. Electro- and Solar-Driven Fuel Synthesis with First Row Transition Metal Complexes. *Chem. Rev.* **2019**, *119*, 2752−2875.

(2) Walter, M. G.; Warren, E. L.; McKone, J. R.; Boettcher, S. W.; Mi, Q.; Santori, E. A.; Lewis, N. S. Solar Water Splitting Cells. *Chem. Rev.* **2010**, *110*, 6446−6473.

DOI: 10.1021/acscatal.9b02984
ACS Catal. 2019, 9, 9530−9538

(3) Tachibana, Y.; Vayssieres, L.; Durrant, J. R. Artificial Photosynthesis for Solar Water-Splitting. *Nat. Photonics* **2012**, *6*, 511−518.
(4) Brennaman, M. K.; Dillon, R. J.; Alibabaei, L.; Gish, M. K.; Dares, C. J.; Ashford, D. L.; House, R. L.; Meyer, G. J.; Papanikolas, J. M.; Meyer, T. J. Finding the Way to Solar Fuels with Dye-Sensitized Photoelectrosynthesis Cells. *J. Am. Chem. Soc.* **2016**, *138*, 13085−13102.
(5) Gibson, E. A. Dye-Sensitized Photocathodes for H_2 Evolution. *Chem. Soc. Rev.* **2017**, *46*, 6194−6209.
(6) Zhang, B.; Sun, L. Artificial Photosynthesis: Opportunities and Challenges of Molecular Catalysts. *Chem. Soc. Rev.* **2019**, *48*, 2216−2264.
(7) Xu, P.; McCool, N. S.; Mallouk, T. E. Water Splitting Dye-Sensitized Solar Cells. *Nano Today* **2017**, *14*, 42−58.
(8) Hennessey, S.; Farràs, P. Production of Solar Chemicals: Gaining Selectivity with Hybrid Molecule/Semiconductor Assemblies. *Chem. Commun.* **2018**, *54*, 6662−6680.
(9) Troian-Gautier, L.; DiMarco, B. N.; Sampaio, R. N.; Marquard, S. L.; Meyer, G. J. Evidence That ΔS‡ Controls Interfacial Electron Transfer Dynamics from Anatase TiO_2 to Molecular Acceptors. *J. Am. Chem. Soc.* **2018**, *140*, 3019−3029.
(10) Xu, P.; Mallouk, T. E. Charge Transfer Dynamics in Aqueous Dye-Sensitized Photoelectrochemical Cells: Implications for Water Splitting Efficiency. *J. Phys. Chem. C* **2019**, *123*, 299−305.
(11) Black, F. A.; Clark, C. A.; Summers, G. H.; Clark, I. P.; Towrie, M.; Penfold, T.; George, M. W.; Gibson, E. A. Investigating Interfacial Electron Transfer in Dye-Sensitized NiO Using Vibrational Spectroscopy. *Phys. Chem. Chem. Phys.* **2017**, *19*, 7877−7885.
(12) D'Amario, L.; Antila, L. J.; Pettersson Rimgard, B.; Boschloo, G.; Hammarström, L. Kinetic Evidence of Two Pathways for Charge Recombination in NiO-Based Dye-Sensitized Solar Cells. *J. Phys. Chem. Lett.* **2015**, *6*, 779−783.
(13) Smeigh, A. L.; Le Pleux, L.; Fortage, J.; Pellegrin, Y.; Blart, E.; Odobel, F.; Hammarström, L. Ultrafast Recombination for NiO Sensitized with a Series of Perylene Imide Sensitizers Exhibiting Marcus Normal Behaviour. *Chem. Commun.* **2012**, *48*, 678−680.
(14) Shan, B.; Farnum, B. H.; Wee, K.-R.; Meyer, T. J. Generation of Long-Lived Redox Equivalents in Self-Assembled Bilayer Structures on Metal Oxide Electrodes. *J. Phys. Chem. C* **2017**, *121*, 5882−5890.
(15) Föhlinger, J.; Maji, S.; Brown, A.; Mijangos, E.; Ott, S.; Hammarström, L. Self-Quenching and Slow Hole Injection May Limit the Efficiency in NiO-Based Dye-Sensitized Solar Cells. *J. Phys. Chem. C* **2018**, *122*, 13902−13910.
(16) Nikolaou, V.; Charisiadis, A.; Charalambidis, G.; Coutsolelos, A. G.; Odobel, F. Recent Advances and Insights in Dye-Sensitized NiO Photocathodes for Photovoltaic Devices. *J. Mater. Chem. A* **2017**, *5*, 21077−21113.
(17) Odobel, F.; Pellegrin, Y. Recent Advances in the Sensitization of Wide-Band-Gap Nanostructured p-Type Semiconductors. Photovoltaic and Photocatalytic Applications. *J. Phys. Chem. Lett.* **2013**, *4*, 2551−2564.
(18) Moore, G. F.; Blakemore, J. D.; Milot, R. L.; Hull, J. F.; Song, H.; Cai, L.; Schmuttenmaer, C. A.; Crabtree, R. H.; Brudvig, G. W. A Visible Light Water-Splitting Cell with a Photoanode Formed by Codeposition of a High-Potential Porphyrin and an Iridium Water-Oxidation Catalyst. *Energy Environ. Sci.* **2011**, *4*, 2389−2392.
(19) Zhang, L.; Favereau, L.; Farré, Y.; Mijangos, E.; Pellegrin, Y.; Blart, E.; Odobel, F.; Hammarström, L. Ultrafast and Slow Charge Recombination Dynamics of Diketopyrrolopyrrole−NiO Dye Sensitized Solar Cells. *Phys. Chem. Chem. Phys.* **2016**, *18*, 18515−18527.
(20) Brown, A. M.; Antila, L. J.; Mirmohades, M.; Pullen, S.; Ott, S.; Hammarström, L. Ultrafast Electron Transfer between Dye and Catalyst on a Mesoporous NiO Surface. *J. Am. Chem. Soc.* **2016**, *138*, 8060−8063.
(21) Gilbert Gatty, M.; Pullen, S.; Sheibani, E.; Tian, H.; Ott, S.; Hammarström, L. Direct Evidence of Catalyst Reduction on Dye and Catalyst Co-Sensitized NiO Photocathodes by Mid- Infrared Transient Absorption Spectroscopy. *Chem. Sci.* **2018**, *9*, 4983−4991.
(22) Borgström, M.; Blart, E.; Boschloo, G.; Mukhtar, E.; Hagfeldt, A.; Hammarström, L.; Odobel, F. Sensitized Hole Injection of Phosphorus Porphyrin into NiO: Toward New Photovoltaic Devices. *J. Phys. Chem. B* **2005**, *109*, 22928−22934.
(23) Morandeira, A.; Boschloo, G.; Hagfeldt, A.; Hammarström, L. Photoinduced Ultrafast Dynamics of Coumarin 343 Sensitized P-Type-Nanostructured NiO Films. *J. Phys. Chem. B* **2005**, *109*, 19403−19410.
(24) Daeneke, T.; Yu, Z.; Lee, G. P.; Fu, D.; Duffy, N. W.; Makuta, S.; Tachibana, Y.; Spiccia, L.; Mishra, A.; Bäuerle, P.; Bach, U. Dominating Energy Losses in NiO P-Type Dye-Sensitized Solar Cells. *Adv. Energy Mater.* **2015**, *5*, 1401387.
(25) Gardner, J. M.; Beyler, M.; Karnahl, M.; Tschierlei, S.; Ott, S.; Hammarström, L. Light-Driven Electron Transfer between a Photosensitizer and a Proton-Reducing Catalyst Co-Adsorbed to NiO. *J. Am. Chem. Soc.* **2012**, *134*, 19322−19325.
(26) Gross, M. A.; Creissen, C. E.; Orchard, K. L.; Reisner, E. Photoelectrochemical Hydrogen Production in Water Using a Layer-by-Layer Assembly of a Ru Dye and Ni Catalyst on NiO. *Chem. Sci.* **2016**, *7*, 5537−5546.
(27) Shan, B.; Das, A. K.; Marquard, S. L.; Farnum, B. H.; Wang, D.; Bullock, R. M.; Meyer, T. J. Photogeneration of Hydrogen from Water by a Robust Dye-Sensitized Photocathode. *Energy Environ. Sci.* **2016**, *9*, 3693−3697.
(28) Shan, B.; Sherman, B. D.; Klug, C. M.; Nayak, A.; Marquard, S. L.; Liu, Q.; Bullock, R. M.; Meyer, T. J. Modulating Hole Transport in Multilayered Photocathodes with Derivatized P-Type Nickel Oxide and Molecular Assemblies for Solar-Driven Water Splitting. *J. Phys. Chem. Lett.* **2017**, *8*, 4374−4379.
(29) Orchard, K. L.; Hojo, D.; Sokol, K. P.; Chan, M.-J.; Asao, N.; Adschiri, T.; Reisner, E. Catechol−TiO_2 Hybrids for Photocatalytic H_2 Production and Photocathode Assembly. *Chem. Commun.* **2017**, *53*, 12638−12641.
(30) Põldme, N.; O'Reilly, L.; Fletcher, I.; Portoles, J.; Sazanovich, I. V.; Towrie, M.; Long, C.; Vos, J. G.; Pryce, M. T.; Gibson, E. A. Photoelectrocatalytic H_2 Evolution from Integrated Photocatalysts Adsorbed on NiO. *Chem. Sci.* **2019**, *10*, 99−112.
(31) Kaeffer, N.; Massin, J.; Lebrun, C.; Renault, O.; Chavarot-Kerlidou, M.; Artero, V. Covalent Design for Dye-Sensitized H_2-Evolving Photocathodes Based on a Cobalt Diimine-Dioxime Catalyst. *J. Am. Chem. Soc.* **2016**, *138*, 12308−12311.
(32) Kumagai, H.; Sahara, G.; Maeda, K.; Higashi, M.; Abe, R.; Ishitani, O. Hybrid Photocathode Consisting of a $CuGaO_2$ p-Type Semiconductor and a Ru(II)−Re(I) Supramolecular Photocatalyst: Non-Biased Visible-Light-Driven CO_2 Reduction with Water Oxidation. *Chem. Sci.* **2017**, *8*, 4242−4249.
(33) Sahara, G.; Kumagai, H.; Maeda, K.; Kaeffer, N.; Artero, V.; Higashi, M.; Abe, R.; Ishitani, O. Photoelectrochemical Reduction of CO_2 Coupled to Water Oxidation Using a Photocathode with a Ru(II)-Re(I) Complex Photocatalyst and a CoOx/TaON Photoanode. *J. Am. Chem. Soc.* **2016**, *138*, 14152−14158.
(34) Kamata, R.; Kumagai, H.; Yamazaki, Y.; Sahara, G.; Ishitani, O. Photoelectrochemical CO_2 Reduction Using a Ru(II)−Re(I) Supramolecular Photocatalyst Connected to a Vinyl Polymer on a NiO Electrode. *ACS Appl. Mater. Interfaces* **2019**, *11*, 5632−5641.
(35) Li, T.-T.; Shan, B.; Meyer, T. J. Stable Molecular Photocathode for Solar-Driven CO_2 Reduction in Aqueous Solutions. *ACS Energy Lett.* **2019**, *4*, 629−636.
(36) Pati, P. B.; Zhang, L.; Philippe, B.; Fernández-Terán, R.; Ahmadi, S.; Tian, L.; Rensmo, H.; Hammarström, L.; Tian, H. Insights into the Mechanism of a Covalently Linked Organic Dye−Cobaloxime Catalyst System for Dye-Sensitized Solar Fuel Devices. *ChemSusChem* **2017**, *10*, 2480−2495.
(37) Bold, S.; Zedler, L.; Zhang, Y.; Massin, J.; Artero, V.; Chavarot-Kerlidou, M.; Dietzek, B. Electron Transfer in a Covalent Dye-Cobalt Catalyst Assembly - a Transient Absorption Spectroelectrochemistry Perspective. *Chem. Commun.* **2018**, *54*, 10594−10597.
(38) Kaeffer, N.; Windle, C. D.; Brisse, R.; Gablin, C.; Leonard, D.; Jousselme, B.; Chavarot-Kerlidou, M.; Artero, V. Insights into the

DOI: 10.1021/acscatal.9b02984
ACS Catal. 2019, 9, 9530−9538

Mechanism and Aging of a Noble-Metal Free H_2-Evolving Dye-Sensitized Photocathode. *Chem. Sci.* **2018**, *9*, 6721−6738.
(39) Haque, S. A.; Handa, S.; Peter, K.; Palomares, E.; Thelakkat, M.; Durrant, J. R. Supermolecular Control of Charge Transfer in Dye-Sensitized Nanocrystalline TiO_2 Films: Towards a Quantitative Structure-Function Relationship. *Angew. Chem., Int. Ed.* **2005**, *44*, 5740−5744.
(40) Hu, K.; Blair, A. D.; Piechota, E. J.; Schauer, P. A.; Sampaio, R. N.; Parlane, F. G. L.; Meyer, G. J.; Berlinguette, C. P. Kinetic Pathway for Interfacial Electron Transfer from a Semiconductor to a Molecule. *Nat. Chem.* **2016**, *8*, 853−859.
(41) Clifford, J. N.; Palomares, E.; Nazeeruddin, M. K.; Grätzel, M.; Nelson, J.; Li, X.; Long, N. J.; Durrant, J. R. Molecular Control of Recombination Dynamics in Dye-Sensitized Nanocrystalline TiO_2 Films: Free Energy vs Distance Dependence. *J. Am. Chem. Soc.* **2004**, *126*, 5225−5233.
(42) Ardo, S.; Meyer, G. J. Photodriven Heterogeneous Charge Transfer with Transition-Metal Compounds Anchored to TiO_2 Semiconductor Surfaces. *Chem. Soc. Rev.* **2009**, *38*, 115−164.
(43) Han, Y.; Dillon, R. J.; Flynn, C. J.; Rountree, E. S.; Alibabaei, L.; Cahoon, J. F.; Papanikolas, J. M.; Dempsey, J. L. Interfacial Electron Transfer Yields in Dye-Sensitized NiO Photocathodes Correlated to Excited-State Dipole Orientation of Ruthenium Chromophores. *Can. J. Chem.* **2018**, *96*, 865−874.
(44) Odobel, F.; Pellegrin, Y.; Gibson, E. A.; Hagfeldt, A.; Smeigh, A. L.; Hammarström, L. Recent Advances and Future Directions to Optimize the Performances of P-Type Dye-Sensitized Solar Cells. *Coord. Chem. Rev.* **2012**, *256*, 2414−2423.
(45) Morandeira, A.; Fortage, J.; Edvinsson, T.; Le Pleux, L.; Blart, E.; Boschloo, G.; Hagfeldt, A.; Hammarström, L.; Odobel, F. Improved Photon-to-Current Conversion Efficiency with a Nanoporous p-Type NiO Electrode by the Use of a Sensitizer-Acceptor Dyad. *J. Phys. Chem. C* **2008**, *112*, 1721−1728.
(46) Swierk, J. R.; Méndez-Hernández, D. D.; McCool, N. S.; Liddell, P.; Terazono, Y.; Pahk, I.; Tomlin, J. J.; Oster, N. V.; Moore, T. A.; Moore, A. L.; Gust, D.; Mallouk, T. E. Metal-Free Organic Sensitizers for Use in Water-Splitting Dye-Sensitized Photoelectrochemical Cells. *Proc. Natl. Acad. Sci. U. S. A.* **2015**, *112*, 1681−1686.
(47) Ooyama, Y.; Harima, Y. Photophysical and Electrochemical Properties, and Molecular Structures of Organic Dyes for Dye-Sensitized Solar Cells. *ChemPhysChem* **2012**, *13*, 4032−4080.
(48) Kirner, J. T.; Finke, R. G. Water-Oxidation Photoanodes Using Organic Light-Harvesting Materials: A Review. *J. Mater. Chem. A* **2017**, *5*, 19560−19592.
(49) Wood, C. J.; Summers, G. H.; Clark, C. A.; Kaeffer, N.; Braeutigam, M.; Carbone, L. R.; D'Amario, L.; Fan, K.; Farré, Y.; Narbey, S.; Oswald, F.; Stevens, L. A.; Parmenter, C. D. J.; Fay, M. W.; La Torre, A.; Snape, C. E.; Dietzek, B.; Dini, D.; Hammarström, L.; Pellegrin, Y.; Odobel, F.; Sun, L.; Artero, V.; Gibson, E. A. A Comprehensive Comparison of Dye-Sensitized NiO Photocathodes for Solar Energy Conversion. *Phys. Chem. Chem. Phys.* **2016**, *18*, 10727−10738.
(50) Gibson, E. A.; Awais, M.; Dini, D.; Dowling, D. P.; Pryce, M. T.; Vos, J. G.; Boschloo, G.; Hagfeldt, A. Dye Sensitised Solar Cells with Nickel Oxide Photocathodes Prepared via Scalable Microwave Sintering. *Phys. Chem. Chem. Phys.* **2013**, *15*, 2411−2420.
(51) Dini, D.; Halpin, Y.; Vos, J. G.; Gibson, E. A. The Influence of the Preparation Method of NiOx Photocathodes on the Efficiency of P-Type Dye-Sensitized Solar Cells. *Coord. Chem. Rev.* **2015**, *304*, 179−201.
(52) Lepleux, L.; Chavillon, B.; Pellegrin, Y.; Blart, E.; Cario, L.; Jobic, S.; Odobel, F. Simple and Reproducible Procedure to Prepare Self-Nanostructured NiO Films for the Fabrication of P-Type Dye-Sensitized Solar Cells. *Inorg. Chem.* **2009**, *48*, 8245−8250.
(53) D'Amario, L.; Föhlinger, J.; Boschloo, G.; Hammarström, L. Unveiling Hole Trapping and Surface Dynamics of NiO Nanoparticles. *Chem. Sci.* **2018**, *9*, 223−230.
(54) D'Amario, L.; Boschloo, G.; Hagfeldt, A.; Hammarström, L. Tuning of Conductivity and Density of States of NiO Mesoporous Films Used in P-Type DSSCs. *J. Phys. Chem. C* **2014**, *118*, 19556−19564.
(55) Mori, S.; Fukuda, S.; Sumikura, S.; Takeda, Y.; Tamaki, Y.; Suzuki, E.; Abe, T. Charge-Transfer Processes in Dye-Sensitized NiO Solar Cells. *J. Phys. Chem. C* **2008**, *112*, 16134−16139.
(56) Li, F.; Fan, K.; Xu, B.; Gabrielsson, E.; Daniel, Q.; Li, L.; Sun, L. Organic Dye-Sensitized Tandem Photoelectrochemical Cell for Light Driven Total Water Splitting. *J. Am. Chem. Soc.* **2015**, *137*, 9153−9159.
(57) Antila, L. J.; Ghamgosar, P.; Maji, S.; Tian, H.; Ott, S.; Hammarström, L. Dynamics and Photochemical H_2 Evolution of Dye−NiO Photocathodes with a Biomimetic FeFe-Catalyst. *ACS Energy Lett.* **2016**, *1*, 1106−1111.
(58) van den Bosch, B.; Rombouts, J. A.; Orru, R. V. A.; Reek, J. N. H.; Detz, R. J. Nickel-Based Dye-Sensitized Photocathode: Towards Proton Reduction Using a Molecular Nickel Catalyst and an Organic Dye. *ChemCatChem* **2016**, *8*, 1392−1398.
(59) Fan, K.; Li, F.; Wang, L.; Daniel, Q.; Gabrielsson, E.; Sun, L. Pt-Free Tandem Molecular Photoelectrochemical Cells for Water Splitting Driven by Visible Light. *Phys. Chem. Chem. Phys.* **2014**, *16*, 25234−25240.
(60) Bredar, A. R. C.; Blanchet, M. D.; Comes, R. B.; Farnum, B. H. Evidence and Influence of Copper Vacancies in P-Type $CuGaO_2$ Mesoporous Films. *ACS Appl. Energy Mater.* **2019**, *2*, 19−28.
(61) Renaud, A.; Chavillon, B.; Le Pleux, L.; Pellegrin, Y.; Blart, E.; Boujtita, M.; Pauporté, T.; Cario, L.; Jobic, S.; Odobel, F. $CuGaO_2$: A Promising Alternative for NiO in p-Type Dye Solar Cells. *J. Mater. Chem.* **2012**, *22*, 14353−14356.
(62) Powar, S.; Xiong, D.; Daeneke, T.; Ma, M. T.; Gupta, A.; Lee, G.; Makuta, S.; Tachibana, Y.; Chen, W.; Spiccia, L.; Cheng, Y. B.; Götz, G.; Bäuerle, P.; Bach, U. Improved Photovoltages for P-Type Dye-Sensitized Solar Cells Using $CuCrO_2$ Nanoparticles. *J. Phys. Chem. C* **2014**, *118*, 16375−16379.
(63) Yu, M.; Draskovic, T. I.; Wu, Y. Cu(I)-Based Delafossite Compounds as Photocathodes in p-Type Dye-Sensitized Solar Cells. *Phys. Chem. Chem. Phys.* **2014**, *16*, 5026−5033.
(64) Creissen, C. E.; Warnan, J.; Reisner, E. Solar H_2 Generation in Water with a $CuCrO_2$ Photocathode Modified with an Organic Dye and Molecular Ni Catalyst. *Chem. Sci.* **2018**, *9*, 1439−1447.
(65) Kuehnel, M. F.; Creissen, C. E.; Sahm, C. D.; Wielend, D.; Schlosser, A.; Orchard, K. L.; Reisner, E. ZnSe Nanorods as Visible-Light Absorbers for Photocatalytic and Photoelectrochemical H_2 Evolution in Water. *Angew. Chem., Int. Ed.* **2019**, *58*, 5059−5063.
(66) Windle, C.; Kumagai, H.; Higashi, M.; Brisse, R.; Bold, S.; Jousselme, B.; Chavarot-Kerlidou, M.; Maeda, K.; Abe, R.; Ishitani, O.; Artero, V. Earth-Abundant Molecular Z-Scheme Photoelectrochemical Cell for Overall Water-Splitting. *J. Am. Chem. Soc.* **2019**, *141*, 9593−9602.
(67) Mersch, D.; Lee, C. Y.; Zhang, J. Z.; Brinkert, K.; Fontecilla-Camps, J. C.; Rutherford, A. W.; Reisner, E. Wiring of Photosystem II to Hydrogenase for Photoelectrochemical Water Splitting. *J. Am. Chem. Soc.* **2015**, *137*, 8541−8549.
(68) Sokol, K. P.; Robinson, W. E.; Warnan, J.; Kornienko, N.; Nowaczyk, M. M.; Ruff, A.; Zhang, J. Z.; Reisner, E. Bias-Free Photoelectrochemical Water Splitting with Photosystem II on a Dye-Sensitized Photoanode Wired to Hydrogenase. *Nat. Energy* **2018**, *3*, 944−951.
(69) Guldin, S.; Hüttner, S.; Kolle, M.; Welland, M. E.; Müller-Buschbaum, P.; Friend, R. H.; Steiner, U.; Tetreault, N. Dye-Sensitized Solar Cell Based on a Three-Dimensional Photonic Crystal. *Nano Lett.* **2010**, *10*, 2303−2309.
(70) Shin, J. H.; Kang, J. H.; Jin, W. M.; Park, J. H.; Cho, Y. S.; Moon, J. H. Facile Synthesis of TiO_2 Inverse Opal Electrodes for Dye-Sensitized Solar Cells. *Langmuir* **2011**, *27*, 856−860.
(71) Lee, S. H. A.; Abrams, N. M.; Hoertz, P. G.; Barber, G. D.; Halaoui, L. I.; Mallouk, T. E. Coupling of Titania Inverse Opals to Nanocrystalline Titania Layers in Dye-Sensitized Solar Cells. *J. Phys. Chem. B* **2008**, *112*, 14415−14421.

DOI: 10.1021/acscatal.9b02984
ACS Catal. 2019, 9, 9530−9538

(72) Lee, J. W.; Lee, J.; Kim, C.; Cho, C. Y.; Moon, J. H. Facile Fabrication of Sub-100nm Mesoscale Inverse Opal Films and Their Application in Dye-Sensitized Solar Cell Electrodes. *Sci. Rep.* **2015**, *4*, 6804.
(73) Tétreault, N.; Grätzel, M. Novel Nanostructures for Next Generation Dye-Sensitized Solar Cells. *Energy Environ. Sci.* **2012**, *5*, 8506−8516.
(74) Leung, J. J.; Vigil, J. A.; Warnan, J.; Edwardes Moore, E.; Reisner, E. Rational Design of Polymers for Selective CO_2 Reduction Catalysis. *Angew. Chem., Int. Ed.* **2019**, *58*, 7697−7701.
(75) Fang, X.; Sokol, K. P.; Heidary, N.; Kandiel, T. A.; Zhang, J. Z.; Reisner, E. Structure-Activity Relationships of Hierarchical Three-Dimensional Electrodes with Photosystem II for Semiartificial Photosynthesis. *Nano Lett.* **2019**, *19*, 1844−1850.
(76) Warnan, J.; Willkomm, J.; Ng, J. N.; Godin, R.; Prantl, S.; Durrant, J. R.; Reisner, E. Solar H_2 Evolution in Water with Modified Diketopyrrolopyrrole Dyes Immobilised on Molecular Co and Ni Catalyst−TiO_2 Hybrids. *Chem. Sci.* **2017**, *8*, 3070−3079.
(77) Warnan, J.; Willkomm, J.; Farré, Y.; Pellegrin, Y.; Boujtita, M.; Odobel, F.; Reisner, E. Solar Electricity and Fuel Production with Perylene Monoimide Dye-Sensitised TiO_2 in Water. *Chem. Sci.* **2019**, *10*, 2758−2766.
(78) Gross, M. A.; Reynal, A.; Durrant, J. R.; Reisner, E. Versatile Photocatalytic Systems for H_2 Generation in Water Based on an Efficient DuBois-Type Nickel Catalyst. *J. Am. Chem. Soc.* **2014**, *136*, 356−366.
(79) Helm, M. L.; Stewart, M. P.; Bullock, R. M.; DuBois, M. R.; DuBois, D. L. A Synthetic Nickel Electrocatalyst with a Turnover Frequency Above 100,000 s^{-1} for H_2 Production. *Science* **2011**, *333*, 863−866.
(80) Shaw, W. J.; Helm, M. L.; DuBois, D. L. A Modular, Energy-Based Approach to the Development of Nickel Containing Molecular Electrocatalysts for Hydrogen Production and Oxidation. *Biochim. Biophys. Acta, Bioenerg.* **2013**, *1827*, 1123−1139.
(81) Rosser, T. E.; Hisatomi, T.; Sun, S.; Antón-García, D.; Minegishi, T.; Reisner, E.; Domen, K. $La_5Ti_2Cu_{0.9}Ag_{0.1}S_5O_7$ Modified with a Molecular Ni Catalyst for Photoelectrochemical H_2 Generation. *Chem. - Eur. J.* **2018**, *24*, 18393−18397.
(82) Leung, J. J.; Warnan, J.; Nam, D. H.; Zhang, J. Z.; Willkomm, J.; Reisner, E. Photoelectrocatalytic H_2 Evolution in Water with Molecular Catalysts Immobilised on p-Si via a Stabilising Mesoporous TiO_2 Interlayer. *Chem. Sci.* **2017**, *8*, 5172−5180.
(83) Xiong, D.; Xu, Z.; Zeng, X.; Zhang, W.; Chen, W.; Xu, X.; Wang, M.; Cheng, Y. B. Hydrothermal Synthesis of Ultrasmall $CuCrO_2$ Nanocrystal Alternatives to NiO Nanoparticles in Efficient p-Type Dye-Sensitized Solar Cells. *J. Mater. Chem.* **2012**, *22*, 24760−24768.
(84) Willkomm, J.; Orchard, K. L.; Reynal, A.; Pastor, E.; Durrant, J. R.; Reisner, E. Dye-Sensitised Semiconductors Modified with Molecular Catalysts for Light-Driven H_2 Production. *Chem. Soc. Rev.* **2016**, *45*, 9−23.
(85) Hoogeveen, D. A.; Fournier, M.; Bonke, S. A.; Fang, X. Y.; Mozer, A. J.; Mishra, A.; Bäuerle, P.; Simonov, A. N.; Spiccia, L. Photo-Electrocatalytic Hydrogen Generation at Dye-Sensitised Electrodes Functionalised with a Heterogeneous Metal Catalyst. *Electrochim. Acta* **2016**, *219*, 773−780.
(86) Kamire, R. J.; Majewski, M. B.; Hoffeditz, W. L.; Phelan, B. T.; Farha, O. K.; Hupp, J. T.; Wasielewski, M. R. Photodriven Hydrogen Evolution by Molecular Catalysts Using Al_2O_3-Protected Perylene-3,4-Dicarboximide on NiO Electrodes. *Chem. Sci.* **2017**, *22*, 32−57.
(87) Farré, Y.; Maschietto, F.; Föhlinger, J.; Wykes, M.; Planchat, A.; Pellegrin, Y.; Blart, E.; Ciofini, I.; Hammarström, L.; Odobel, F. Manuscript in preparation.
(88) Würthner, F.; Saha-Möller, C. R.; Fimmel, B.; Ogi, S.; Leowanawat, P.; Schmidt, D. Perylene Bisimide Dye Assemblies as Archetype Functional Supramolecular Materials. *Chem. Rev.* **2016**, *116*, 962−1052.
(89) Martindale, B. C. M.; Hutton, G. A. M.; Caputo, C. A.; Reisner, E. Solar Hydrogen Production Using Carbon Quantum Dots and a Molecular Nickel Catalyst. *J. Am. Chem. Soc.* **2015**, *137*, 6018−6025.
(90) Martindale, B. C. M.; Joliat, E.; Bachmann, C.; Alberto, R.; Reisner, E. Clean Donor Oxidation Enhances the H_2 Evolution Activity of a Carbon Quantum Dot-Molecular Catalyst Photosystem. *Angew. Chem., Int. Ed.* **2016**, *55*, 9402−9406.
(91) Ji, Z.; He, M.; Huang, Z.; Ozkan, U.; Wu, Y. Photostable P-Type Dye-Sensitized Photoelectrochemical Cells for Water Reduction. *J. Am. Chem. Soc.* **2013**, *135*, 11696−11699.
(92) Buesen, D.; Hoefer, T.; Zhang, H.; Plumeré, N. A Kinetic Model for Redox-Active Film Based Biophotoelectrodes. *Faraday Discuss.* **2019**, *215*, 39−53.
(93) Ketir, W.; Saadi, S.; Trari, M. Physical and Photoelectrochemical Characterization of $CuCrO_2$ Single Crystal. *J. Solid State Electrochem.* **2012**, *16*, 213−218.
(94) Queffélec, C.; Petit, M.; Janvier, P.; Knight, D. A.; Bujoli, B. Surface Modification Using Phosphonic Acids and Esters. *Chem. Rev.* **2012**, *112*, 3777−3807.
(95) Yu, Y.; Chien, S.-C.; Sun, J.; Hettiaratchy, E. C.; Myers, R. C.; Lin, L.-C.; Wu, Y. Excimer-Mediated Intermolecular Charge Transfer in Self-Assembled Donor-Acceptor Dyes on Metal Oxides. *J. Am. Chem. Soc.* **2019**, *141*, 8727−8731.
(96) Hoogeveen, D. A.; Fournier, M.; Bonke, S. A.; Nattestad, A.; Mishra, A.; Bäuerle, P.; Spiccia, L.; Mozer, A. J.; Simonov, A. N. Origin of Photoelectrochemical Generation of Dihydrogen by a Dye-Sensitized Photocathode without an Intentionally Introduced Catalyst. *J. Phys. Chem. C* **2017**, *121*, 25836−25846.
(97) D'Amario, L.; Jiang, R.; Cappel, U. B.; Gibson, E. A.; Boschloo, G.; Rensmo, H.; Sun, L.; Hammarström, L.; Tian, H. Chemical and Physical Reduction of High Valence Ni States in Mesoporous NiO Film for Solar Cell Application. *ACS Appl. Mater. Interfaces* **2017**, *9*, 33470−33477.
(98) Flynn, C. J.; McCullough, S. M.; Oh, E.; Li, L.; Mercado, C. C.; Farnum, B. H.; Li, W.; Donley, C. L.; You, W.; Nozik, A. J.; McBride, J. R.; Meyer, T. J.; Kanai, Y.; Cahoon, J. F. Site-Selective Passivation of Defects in NiO Solar Photocathodes by Targeted Atomic Deposition. *ACS Appl. Mater. Interfaces* **2016**, *8*, 4754−4761.

DOI: 10.1021/acscatal.9b02984
ACS Catal. 2019, 9, 9530−9538